ELSEVIER

Journal of Photochemistry and Photobiology A: Chemistry 141 (2001) 69–78

Journal of Photochemistry and Photobiology A:Chemistry

www.elsevier.nl/locate/jphotochem

Photomineralisation kinetics of aqueous chlorophenols at a supported TiO_2 surface studied by the channel-flow method with electrochemical detection

Samina Ahmed, Terence J. Kemp*, Patrick R. Unwin*

Department of Chemistry, University of Warwick, Coventry CV4 7AL, UK

Received 15 February 2001; received in revised form 26 March 2001; accepted 28 March 2001

Abstract

The channel flow method with electrochemical detection (CFMED) of Cl^- ion product has been applied to the photodegradation kinetics of four chlorophenols (CPs) undergoing photolysis ($\lambda > 300$ nm) at a TiO_2 film. The effects on the rate of photomineralisation of (i) varying CP concentration, (ii) O_2 concentration, (iii) flow rate, (iv) light intensity and (v) supporting electrolyte, have been examined. Of particular note are the accelerative effects of increasing $[O_2]$ and removing background electrolyte. The kinetics have been shown to fit models derived from Langmuir–Hinshelwood kinetics; at high [CP], the rates fit a surface-limited model, but at low [CP], this model proves inadequate and a mixed-control model, incorporating mass transfer as an additional parameter, is shown to be necessary. The approach developed allows the conditions under which mass transfer is important in controlling photomineralisation rates to be identified.

Keywords: Channel flow method; Electrochemical detection; Thin-film reactor; Chlorophenol; TiO_2; Photomineralisation; Mass transfer

1. Introduction

The application of UV-irradiated semiconductors, particularly TiO_2, to the mineralisation of a range of toxic organic materials, particularly in aqueous solution, has been the subject of intense study, resulting in hundreds of publications and a series of review articles [1–5]. The semiconductor, the band gap of which must fall in the 'useful' UV range of ca. 280–400 nm [3], is usually applied either in the form of a slurry [6–9] or as a thin-film [10–13] deposited on glass or other surfaces (beads, helices, tubes [11], plates). It is generally accepted that the initial photoexcitation results in generation of a hole–electron pair (h^+, e^-) in the semiconductor; both species are located at the semiconductor surface and can function as oxidant and reductant, respectively, in their initial form towards the pollutant substrate (SH) or go on to react with water, in the case of h^+, or with dissolved oxygen [8,11] in the case of e^-

$$h^+ + 2H_2O \rightarrow {}^{\bullet}OH + H_3O^+ \quad (1)$$

$$e^- + O_2 \rightarrow O_2^{\bullet -} \quad (2)$$

Both $^{\bullet}OH$ and $O_2^{\bullet -}$ then attack SH or engage in other bimolecular processes [8] to form H_2O_2.

Kinetic studies of photomineralisation have concentrated on the roles of the semiconductor (nature [3,8], surface area, dopants, catalysis [8]), the substrate SH (nature and concentration [11]), and illumination [14–17] (intensity [14,15], flux density [16], frequency range [17], intermediates [18]). In contrast, the role of mass transport for immobilised systems is only just beginning to be studied [19,20], despite indications of the importance of this parameter more than ten years ago [21]. Thus, the rate of degradation of 4-chlorophenol (4-CP) was recently investigated in a stirred reactor where mass transport was considered to be sufficiently high to have a negligible effect on the rate [19]. In a preliminary study of the photodegradation kinetics of 4-CP at TiO_2, we used the channel flow method combined with electrochemical detection (CFMED) [20] to resolve surface kinetics and mass transport effects [21,22]. In the present paper, we extend this approach to additional monochlorophenols and a dichlorophenol (2-CP, 3-CP, 2,4-DCP), and explore the effects of varying CP concentration, light intensity, oxygen concentration and adding supporting electrolyte.

* Corresponding authors. Fax: +44-2476524112.
E-mail addresses: t.j.kemp@warwick.ac.uk (T.J. Kemp), p.r.unwin@warwick.ac.uk (P.R. Unwin).

1010-6030/01/$ – see front matter
PII: S1010-6030(01)00434-8

2. Experimental

2.1. Chemicals

All solutions were prepared using Milli-Q water (resistivity 18 MΩ cm), and contained a particular CP at the concentration specified herein. The substrates 2-CP (98%) and 3-CP (99%) were obtained from Lancaster (UK), while 4-CP and 2,4-DCP (both 99%) were from Aldrich (UK). For some experiments, solutions also contained sodium perchlorate (Analar, BDH, UK) at the concentrations specified later. Previous workers have used KNO_3 to control ionic strength [18].

2.2. Film preparation

The TiO_2 film was prepared from a Degussa P25 suspension [23], where 5 g of TiO_2 was mixed with 100 cm^3 Milli-Q water, sonicated for 1 h and stirred for 5 h with a magnetic stirrer. The suspension was dropped onto the glass surface of the coverplate (described below) and then dried with Ar gas. This process was typically repeated five times, to achieve an even, complete coating. The coverplate was dried in an oven at 373 K for 12 h, resulting in a mechanically stable film.

2.3. Light source

A high powered xenon lamp (Illuminator 6000, Eurosep Instruments, Cergy-Pontoise, France) was used as the source of UV-irradiation. The intensity of the lamp was determined following a modification of the method developed by Hatchard and Parker [24], and a full emittance profile has been determined [17].

2.4. Channel-flow instrumentation

The instrumentation for these studies was described in our preliminary paper [20]. In brief, the home-built channel flow cell employed for the interfacial photoelectrochemical studies was a combination of three detachable parts (Fig. 1): (i) a channel inlet–outlet unit with a quartz window to permit illumination; (ii) a coverplate containing the reference and indicator (detector) electrodes together with a glass slide on which the TiO_2 film was deposited and (iii) a Teflon spacer.

The channel inlet–outlet unit was 6.0 cm in length, 4.0 cm in width and 1.0 cm in height, and was constructed from PVC. Inlet and outlet ports were drilled at both ends of the cell to facilitate the flow of solution. The pressure across the channel width was minimised by setting two ducts (7.5 mm × 3.0 mm with a depth of 3.0 mm) centrally in the cell at a distance of 4.0 cm apart but adjacent to the ports. The quartz window (1.2 cm × 1.0 cm) was positioned 2.6 cm from the upstream edge and 1.8 cm from the downstream edge of the cell and secured with silicone adhesive (Dow Corning 3140 RTV coating). When the flow cell was assembled, the quartz window was just over the TiO_2 substrate of the coverplate, allowing UV-illumination of the photocatalyst.

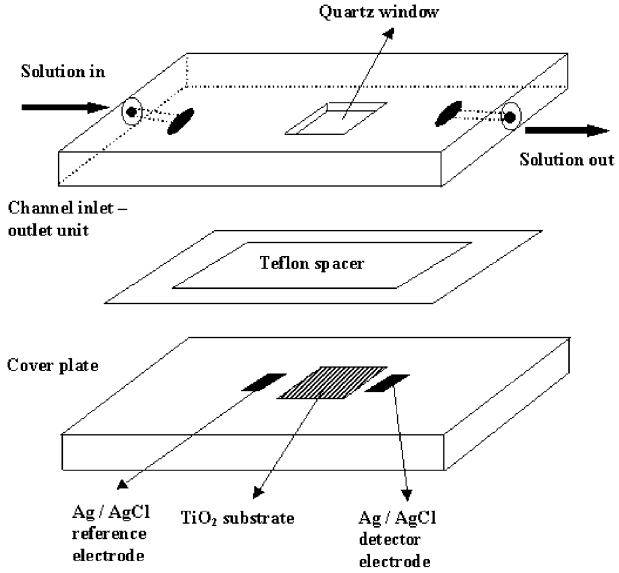

Fig. 1. Schematic of the channel flow cell employed to study the photodegradation of chlorophenols.

The coverplate, of similar dimensions to the channel inlet–outlet unit, was cast from epoxy resin (CY21 resin and HY139 hardener, Delta Resin Ltd., Stockport, mixed at a ratio of 3:1, respectively) using a detachable Teflon mould. A glass slide (1.20 cm × 1.0 cm) was placed in the coverplate (onto which TiO_2 film was deposited). The indicator (detector) electrode was positioned 2.0 mm from the downstream edge of the glass slide, while the reference electrode was 8.0 mm from the upstream edge.

Two Ag band electrodes, 0.25 mm in length (measured along the cell) and 4.0 mm wide (across the cell) were coated in AgCl via the oxidation of 0.1 mol dm^{-3} KCl solution, as described previously [20] and served as the reference and indicator electrodes. The width of the indicator electrode was much smaller than the channel width (12.0 mm) to avoid possible interference from any viscous effects on the flow at the channel edge. The coverplate was polished and prepared prior to experiments, as described previously [20]. The spacer was cut from a 0.5 mm thick Teflon sheet (Goodfellow, Cambridge, UK) and reflected the internal channel dimensions, producing a rectangular duct 45 mm long and 12 mm wide. The thickness of the Teflon spacer represented the channel height.

All these three parts were sealed together using six bolts at the edges of both the channel unit and the coverplate, with careful positioning of the Teflon spacer providing a leak-proof channel flow cell. When the cell was assembled, the electrodes were in the shadow of the PVC plate, ensuring that there was no illumination of the electrode surfaces. The complete flow cell was then clamped vertically to avoid any bubble formation in the system and flow was achieved using

gravimetric feed system as described previously [20]. For experiments under 1 atm of O_2, the solution in the feed reservoir was purged with O_2 (99.5% purity, BOC) and the flow tubing (1.5 mm i.d., Anachem, Luton) was jacketed with PVC tubing (12 mm i.d.) through which O_2 was also passed.

The photodegradation kinetics were monitored via the formation of Cl^-, determined by recording the potential difference (Keithley 175 Autoranging Multimeter) between the downstream (indicator) and upstream (reference) electrodes. Although the in-flowing solution did not contain Cl^-, the upstream electode maintained a constant reference potential over all of the flow rates investigated, presumably due to the rapid dissolution kinetics of AgCl, ensuring that the upstream electrode was always in contact with a locally saturated solution of sparingly soluble salt. Similar results were obtained when a saturated calomel electrode was employed as a reference electrode in the reservoir of the flow system. The measured potential difference was converted to Cl^- using a calibration plot, as described previously [20]. When the lamp was switched off, no detectable levels of Cl^- were produced by the flow of the aqueous chlorophenols over the TiO_2 film.

2.5. Batch photoreactor studies

The batch photoreactor used in this study was as described previously [16]. An aqueous solution of 1.0×10^{-3} mol dm^{-3} 4-CP (with or without supporting electrolyte) was suspended with 0.1% TiO_2 and sonicated for ca. 15 min. The solution containing suspended TiO_2 was then purged with compressed air for 10 min prior to the illumination and purging was continued during illumination to maintain a suspension of TiO_2. An Ag/AgCl detector electrode (protected from direct illumination) and a saturated calomel electrode, which served as a reference electrode, were dipped into the suspension and the formation of Cl^- was monitored as a function of time, during illumination, using the digital multimeter.

3. Results and discussion

3.1. Formulation of models

The key product for CFMED in the photomineralisation of CPs is Cl^- ion, and modelling of its formation kinetics is the heart of our methodology.

The photomineralisation process is generally explained by invoking a Langmuir–Hinshelwood kinetic scheme [1,18,19]

$$\text{rate} = \frac{\gamma K_{O_2}[O_2] I_a^m K_{CP}[CP]}{(1 + K_{O_2}[O_2])(1 + K_{CP}[CP])} \tag{3}$$

where K_{O_2} and K_{CP} are the equilibrium adsorption constants for O_2 and CP, respectively, at the TiO_2 surface, I_a the light flux, m a power term (varying between 0.5 and 1.0), and γ a proportionality constant. This rate law has already been verified in numerous cases of photodegradation studies in suspensions [1]. However, for immobilised catalytic processes, a quantitative description is needed considering the possible involvement of the mass transport effects.

Eq. (3) was treated at two simplified levels. At the simplest level, it was assumed that there was no depletion of either O_2 or the CP under study at the TiO_2 surface. In this case, Eq. (3) can be simplified, first by considering the fraction of sites covered by the CP of interest and O_2 as follows:

$$\frac{K_{CP}[CP]}{1 + K_{CP}[CP]} = \theta_{CP} \tag{4}$$

$$\frac{K_{O_2}[O_2]}{1 + K_{O_2}[O_2]} = \theta_{O_2} \tag{5}$$

The term γI_a^m can be expressed as a light-intensity-dependent heterogeneous rate constant for surface-limited conditions

$$k_{SL} = \gamma I_a^m \tag{6}$$

where k_{SL} has units of mol cm^{-2} s^{-1}.

Combination of the above three equations provides a simplified version of Eq. (3), which we refer to as the surface-limited model.

$$\text{rate} = k_{SL}\theta_{SP}\theta_{O_2} = k'_{SL} \tag{7}$$

The second level approximation was to consider the reaction under mixed transport–kinetic control. If transport of CP to the TiO_2 surface is considered as an important factor (without any change of the interfacial concentration of O_2 from that in the bulk solution), then the rate law for this mixed-control model can be written as

$$\text{rate} = k_{MC}\theta_{O_2}\frac{K_{CP}[CP]_i}{1 + K_{CP}[CP]_i} = \frac{k'_{MC}K_{CP}[CP]_i}{1 + K_{CP}[CP]_i} \tag{8}$$

where the subscript 'i' denotes the solution concentration of CP adjacent to the TiO_2/aqueous interface and

$$k'_{MC} = k_{MC}\theta_{O_2} \tag{9}$$

The well-defined mass transport of the channel flow method enabled local concentrations of Cl^- at the detector electrode to be calculated as a function of flow rate, geometry and kinetics for each of the two candidate rate laws. With reference to the co-ordinate system in Fig. 2, the transport of Cl^- (in both the surface-limited and mixed-control models) and CP (in the mixed-control model only), under steady-state conditions, is governed by

$$D_{CP}\frac{\partial^2[CP]}{\partial y^2} = v_0\left[1 - \frac{(y-h)^2}{h^2}\right]\frac{\partial[CP]}{\partial x} \tag{10}$$

$$D_{Cl^-}\frac{\partial^2[Cl^-]}{\partial y^2} = v_0\left[1 - \frac{(y-h)^2}{h^2}\right]\frac{\partial[Cl^-]}{\partial x} \tag{11}$$

The x and y co-ordinates are defined in Fig. 2. D_i denotes the diffusion coefficient of species i (Cl^- or CP) and v_0 is

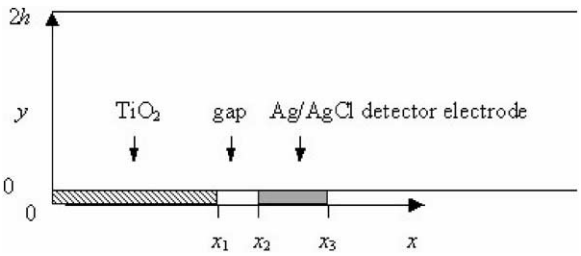

Fig. 2. Co-ordinate system for CFMED simulations.

the fluid velocity in the centre of the channel. This latter variable is related to the volume flow rate, V_f, and geometry of the channel cell by

$$v_0 = \frac{3V_f}{4hd} \tag{12}$$

where h is the channel half-height and d the channel width.

The two rate laws embodied in Eqs. (7) and (8) form the boundary conditions at the TiO_2 surface for the two models of interest

$$y = 0,\ 0 \le x < x_1: \quad -D_{Cl^-}\frac{\partial[Cl^-]}{\partial y} = k'_{SL} \tag{13}$$

$$D_{CP}\frac{\partial[CP]}{\partial y} = -D_{Cl^-}\frac{\partial[Cl^-]}{\partial y} = k'_{MC}\frac{K_{CP}[CP]_{y=0}}{1 + K_{CP}[CP]_{y=0}} \tag{14}$$

Additional boundary conditions for the other walls and the non-reactive zones of the channel are

$$y = 0,\ x_1 < x \le x_3: \quad D_{CP}\frac{\partial[CP]}{\partial y} = D_{Cl^-}\frac{\partial[Cl^-]}{\partial y} = 0 \tag{15}$$

$$y = 2h,\ \text{all}\ x: \quad D_{CP}\frac{\partial[CP]}{\partial y} = D_{Cl^-}\frac{\partial[Cl^-]}{\partial y} = 0 \tag{16}$$

and

$$x < 0,\ \text{all}\ y: \quad [Cl^-] = 0, \qquad [CP] = [CP]^* \tag{17}$$

where the asterisk (*) in superscript represents the bulk concentration.

The problem outlined was solved using the backwards implicit finite difference method (BIFDM), which has been applied extensively to steady-state CFMED problems [25–27]. For a given cell geometry (cm), [CP] in mol cm^{-3}, volume flow rate (cm^3 s^{-1}) and rate constant (mol cm^{-2} s^{-1}) for the heterogeneous process, the simulation provided values for [Cl$^-$] at the downstream electrode, for the two models, which could then be compared to the experimental data.

The complete mineralisation process results in the formation of CO_2, H_2O and HCl, but with various intermediates produced in the degradation of a particular substituted chlorophenol compound. The involvement of intermediates and the timescales for their production have been detailed for batch sensitised processes [28–30]. In the present study, with a continuous flow system, reactants are continuously flowed over the TiO_2 catalyst and intermediates rapidly transported to waste. The rates of Cl$^-$ formation are thus *initial* rates for the degradation of a CP. Thus, the two models developed here for the numerical simulation of the [Cl$^-$] presume one Cl$^-$ ion is expelled per CP molecule, even for 2,4-DCP as batch studies [27] show the second Cl atom is lost relatively slowly.

Table 1
Equilibrium adsorption constants (K_{CP}) for CPs on TiO_2

CPs	K_{CP} (dm^3 mol^{-1})	Reference
4-CP	4.9×10^3, $(29 \pm 3) \times 10^3$	[33,29]
3-CP	1.6×10^3	[34]
2-CP	3.6×10^3	[9,35]
2,4-DCP	3.2×10^3	[28]

The literature value [31] for $D_{Cl^-} = 1.9 \times 10^{-5}$ cm^2 s^{-1} was used for the surface-limited and mixed-control models, while for the mixed-control model, the values for D_{CP} were calculated as 0.94×10^{-5} cm^2 s^{-1} for the monochlorophenols and 0.86×10^{-5} cm^2 s^{-1} for 2,4-DCP using the Wilke–Chang correlation [32]. Literature values [28,33–35] for the equilibrium adsorption constants of the chlorophenols, as listed in Table 1, were initially considered.

For 4-CP, values of K_{CP} up to 30.0×10^3 M^{-1} have been reported for studies in suspensions [28], but this value did not provide a good description of the experimental results presented later; the lower value employed in Table 1 is considered to be appropriate to thin-film systems [33].

To illustrate the different behaviour predicted by the models, Fig. 3 shows [Cl$^-$] at a detector electrode simulated for the mixed-control and surface-limited cases for 5.0×10^{-4} mol dm^{-3} 4-CP solution as a model substrate. A typical rate constant of $k'_{MC} = 1.0 \times 10^{-10}$ mol cm^{-2} s^{-1} was

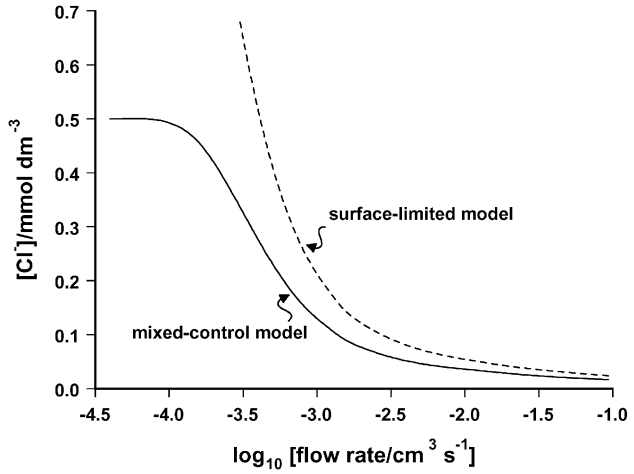

Fig. 3. Theoretical simulations of the mixed-control (solid line) and surface-limited (dashed line) models for 5.0×10^{-4} mol dm^{-3} 4-CP. The estimated rate constants, k'_{MC} and k'_{SL} for the mixed-control and surface-limited models, respectively, were 1.0×10^{-10} and 7.1×10^{-11} mol cm^{-2} s^{-1}. The spacer height was 0.5 mm, with the other parameters cited in the text.

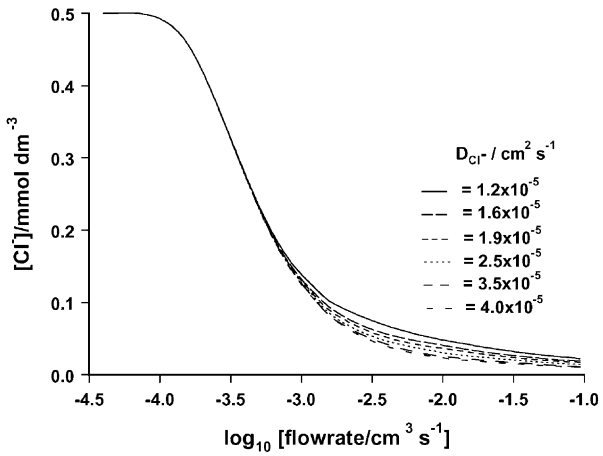

Fig. 4. Theoretical simulations of the mixed-control model ($k'_{MC} = 1.0 \times 10^{-10}$ mol cm^{-2} s^{-1}) for 5.0×10^{-4} mol dm^{-3} 4-CP with variation of the values of D_{Cl^-} over the range of 1.2×10^{-5}–4.0×10^{-5} cm^2 s^{-1}. The spacer height was 0.5 mm.

considered. If depletion of CP is unimportant, this corresponds to $k'_{SL} = 7.1 \times 10^{-11}$ mol cm^{-2} s^{-1} (cf. Eqs. (7) and (8)). Standard cell parameters were as follows: interface length 1.395 cm; width 1.340 cm; detector electrode length 0.025 cm; gap between the end of the interface and the detector electrode 0.205 cm; channel height 0.050 cm and channel width 1.460 cm. These numerical simulations show that the mixed-control model, embodied in Eq. (13), predicts the calculated [Cl$^-$] to level off towards [CP]* at low flow rate whereas in this regime, for the surface-limited model, [Cl$^-$] increases without limit, which is clearly unrealistic. Only at the very highest flow rates do the two models converge, i.e. at $V_f > 0.1$ cm^3 s^{-1}.

Although the value of $D_{Cl^-} = 1.9 \times 10^{-5}$ cm^2 s^{-1} was used for this study, for experiments with no supporting electrolyte, the effective diffusion coefficient of Cl$^-$ will depend on the counter cation, which is unknown under the conditions of the experiments. Thus, simulations were also carried out for the mixed-control model considering variation of the value of D_{Cl^-} over the maximum possible range of 1.2×10^{-5}–4.0×10^{-5} cm^2 s^{-1} for 5.0×10^{-4} mol dm^{-3} 4-CP solutions. A rate constant $k'_{MC} = 1.0 \times 10^{-10}$ mol cm^{-2} s^{-1} was considered with an identical cell geometry to that defined above. Overall, simulated results (Fig. 4) show that variation of D_{Cl^-} has a relatively minor effect on the calculated detector electrode response, under the conditions of interest.

3.2. Photodegradation of 4-CP by CFMED

3.2.1. Effect of 4-CP concentration

The trends of the degradation kinetics with bulk 4-CP concentration are readily explained by referring to the observed Cl$^-$ ion concentration at the detector electrode during the photomineralisation of 5.0×10^{-3}–2.0×10^{-4} mol dm^{-3} 4-CP under aerated conditions with a light

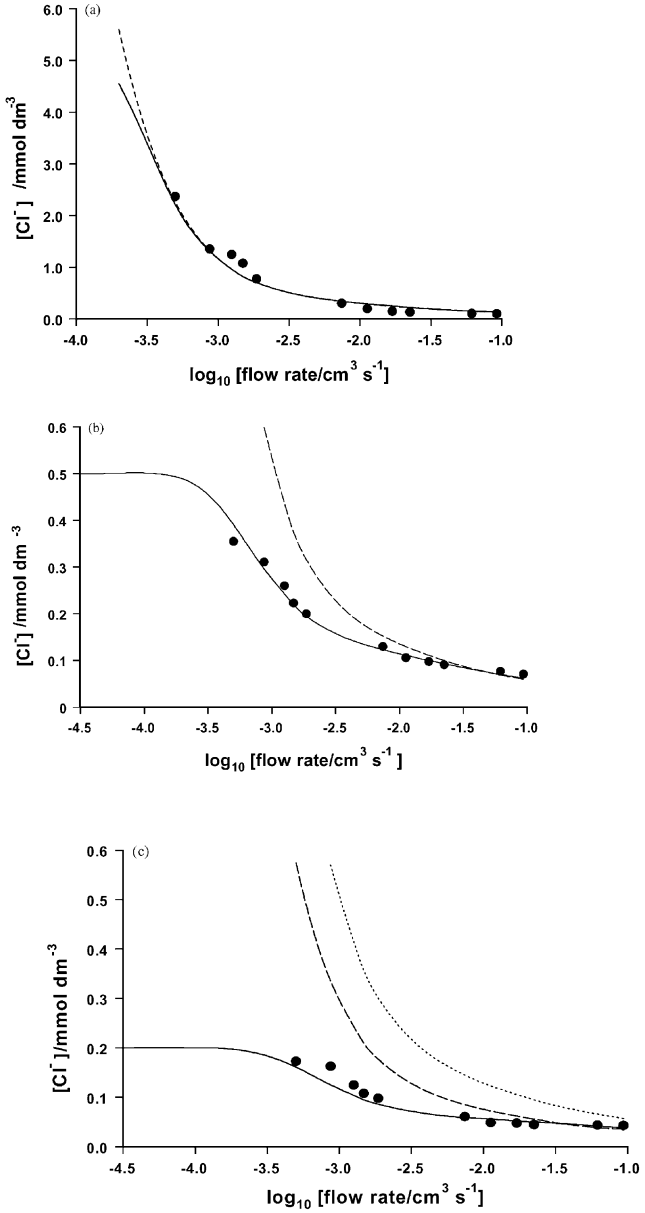

Fig. 5. [Cl$^-$] at the downstream detector electrode (●) as a function of $\log_{10}$ (flow rate) for (a) 5.0×10^{-3} mol dm^{-3} 4-CP solution (aerated). The best fits are shown for the mixed-control model (solid line, with $k'_{MC} = 5.8 \times 10^{-10}$ mol cm^{-2} s^{-1}) and the surface-limited model (dashed line, with $k'_{SL} = 5.5 \times 10^{-10}$ mol cm^{-2} s^{-1}). (b) 5.0×10^{-4} mol dm^{-3} 4-CP solution (aerated). The best fits are shown for $k'_{MC} = 4.1 \times 10^{-10}$ mol cm^{-2} s^{-1} (solid line) and $k'_{SL} = 2.5 \times 10^{-10}$ mol cm^{-2} s^{-1} (dashed line). (c) 2.0×10^{-4} mol dm^{-3} 4-CP solution (aerated). The best fits are shown for $k'_{MC} = 4.8 \times 10^{-10}$ mol cm^{-2} s^{-1} (solid line) and $k'_{SL} = 1.4 \times 10^{-10}$ mol cm^{-2} s^{-1} (dashed line). The behaviour with $k'_{SL} = 2.38 \times 10^{-10}$ mol cm^{-2} s^{-1} is shown as the dotted line.

flux density of 2.0×10^{17} q cm^{-2} s^{-1}. After converting the measured potential difference responses to [Cl$^-$] at the downstream Ag/AgCl indicator electrode, the respective data were obtained for individual bulk concentrations, [4-CP]*, of interest, as shown in Fig. 5a–c.

The experimental results are compared alongside the best fits for the two models developed. These data

clearly indicate that for the higher concentration of 4-CP (5.0×10^{-3} mol dm^{-3}) both of the models fit the experimental data with reasonable agreement over the entire range of flow rates studied. This is because with a high substrate concentration, the relative extent to which 4-CP is consumed at the surface is quite small so that $[CP]_i$ approaches [4-CP]* and the surface-limited model thus provides a good description of the kinetics. In contrast, the results for the more dilute (5.0×10^{-4} and 2.0×10^{-4} mol dm^{-3}) 4-CP solutions conform more closely to the mixed-control model, over the whole range of flow rates considered, because now the relative extent of 4-CP depletion is more significant, particularly as the flow rate is decreased. This pattern of behaviour is consistent with a rate law where the effective order of the reaction with respect to the candidate solution reactant is less than unity [25] as for Eq. (11).

In fitting the data in Fig. 5 to the surface-limited model, the aim was to achieve at least a match in the high flow rate limit, where this model is most appropriate, as discussed earlier (Fig. 3). The deviation of the surface-limited model for lower substrate concentrations clearly points to the enhanced role of the mass transport effect in controlling the overall rate. The expected importance of mass transport effects for dilute solutions was also highlighted by Turchi and Ollis [21]. Accordingly, it is interesting to use the value of k'_{MC} deduced to simulate the behaviour that would be expected if there was no depletion of 4-CP at the TiO_2 surface, i.e. a true surface-limited process. The rate constant (k''_{SL}, mol cm^{-2} s^{-1}) for this case was obtained from

$$k''_{SL} = \frac{k'_{MC} K_{CP}[CP]^*}{1 + K_{CP}[CP]^*} \quad (18)$$

Using the values cited above, $k''_{SL} = 2.38 \times 10^{-10}$ mol cm^{-2} s^{-1} was obtained for the case in Fig. 5c. When this is used to simulate the behaviour, a notably poor fit (dotted line in Fig. 5c) compared to the experimental data is obtained. This re-emphasises the point that there is a range of practically important conditions where mass transport plays a significant role in controlling the kinetics of the process.

Table 2 summarises values of k'_{MC} and k'_{SL} used to obtain the best fit simulations compared to the experimental data for the range of [4-CP]* investigated. In the limit where there is no depletion at the surface, we can write from Eqs. (7) and (8)

$$\frac{1}{k'_{SL}} = \frac{1}{k'_{MC} K_{CP}[CP]^*} + \frac{1}{k'_{MC}} \quad (19)$$

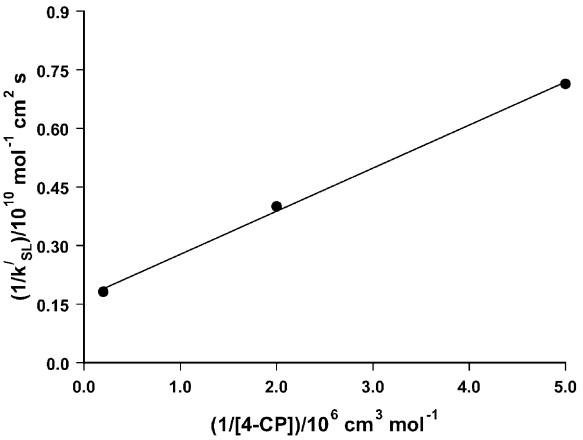

Fig. 6. Analysis of the data derived from Fig. 5 in terms of Eq. (19).

A plot of $1/k'_{SL}$ versus 1/[4-CP]* (Fig. 6), then yields an apparent equilibrium adsorption constant for 4-CP under the present experimental conditions and k'_{MC}. The calculated value for the apparent equilibrium adsorption constant is 1.5×10^3 M^{-1} and $k'_{MC} = 5.9 \times 10^{-10}$ mol cm^{-2} s^{-1}. The value of K_{CP} is in close agreement with the value 1.7×10^3 M^{-1} deduced by Mills and Wang [19] for a thin-film system, but a little lower than used to analyse the data in Fig. 5. On the other hand, k'_{MC} is higher than the mean value deduced from the curve fitting analysis. This is probably because even at the highest flow rates considered in each of Fig. 5a–c, there is some depletion of [4-CP] from the bulk value. This will become increasingly important at lower substrate concentration and so the analysis of Eq. (19) should only be considered as approximate as it will tend to underestimate K_{CP}.

3.2.2. Effect of light intensity

It is well established that the photomineralisation rate depends on the intensity of the incident light [2,14–17]. Accordingly, the influence of the light flux density was investigated by reducing it to 7.2×10^{16} q cm^{-2} s^{-1} for dilute substrate concentrations (5.0×10^{-4} and 2.0×10^{-4} mol dm^{-3} 4-CP) where mass transport has been shown to be a key parameter governing the mineralisation kinetics under the defined experimental conditions. The predicted rate constants providing the best fit for 5.0×10^{-4} mol dm^{-3} 4-CP was $k'_{MC} = 1.5 \times 10^{-10}$ mol cm^{-2} s^{-1}, while for 2.0×10^{-4} M 4-CP solution, the best fit resulted with $k'_{MC} = 1.7 \times 10^{-10}$ mol cm^{-2} s^{-1}. Comparison of these rate constants with those obtained with the same substrate

Table 2
Values of k'_{MC} and k'_{SL} used for the best fit simulations of the theoretical models

[4-CP] (mol dm^{-3})	[O_2] (kPa)	Light flux density (q cm^{-2} s^{-1})	k'_{MC} (mol cm^{-2} s^{-1})	k'_{SL} (mol cm^{-2} s^{-1})
5.0×10^{-3}	20	2.0×10^{17}	5.8×10^{-10}	5.5×10^{-10}
5.0×10^{-4}	20	2.0×10^{17}	4.1×10^{-10}	2.5×10^{-10}
2.0×10^{-4}	20	2.0×10^{17}	4.8×10^{-10}	1.4×10^{-10}

concentrations at higher light flux (Fig. 5) suggests that under aerated solution conditions, the apparent rate constant is closely proportional to the intensity, as found by Mills and Wang [19], who did more extensive studies.

3.2.3. Effect of [O_2]

The presence of higher levels of O_2 speeds up the surface photomineralisation process by scavenging the photogenerated electrons at the TiO_2 surface, producing superoxide anions. Accordingly, the degradation kinetics were also examined under conditions where the level of O_2 in 2.0×10^{-4} mol dm^{-3} 4-CP solution was increased from atmospheric to saturated levels at a light flux of 7.2×10^{16} q cm^{-2} s^{-1}. The experimental results were compared to the best fits to the theoretical models, obtained with $k'_{MC} = 4.5 \times 10^{-10}$ mol cm^{-2} s^{-1} and $k'_{SL} = 1.5 \times 10^{-10}$ mol cm^{-2} s^{-1} (Fig. 7). Again, from the poor fit of the surface-limited approach, the role of mass transport in photomineralisation kinetics is clear over the whole range of flow rates considered.

Comparing the results obtained under these conditions, with those for the same [4-CP]* and light intensity but with an aerated solution, demonstrates that increasing the concentration of O_2 in solution increases k'_{SL} by a factor of 2.5. This type of effect has been seen previously for both immobilised systems [19] and TiO_2 in suspension [12].

3.2.4. Effect of supporting electrolyte

After highlighting the significance of the mass transport effect as a key parameter in controlling the degradation kinetics of 4-CP (in the absence of supporting electrolyte), the next approach was to address the case where the supporting electrolyte is present in excess over the organic substrate. Accordingly, the kinetics of 5.0×10^{-3} and 1.0×10^{-3} mol dm^{-3} 4-CP mineralisation (under aerated conditions) in the presence of 0.1 mol dm^{-3} $NaClO_4$ as supporting electrolyte were analysed (Fig. 8a and b).

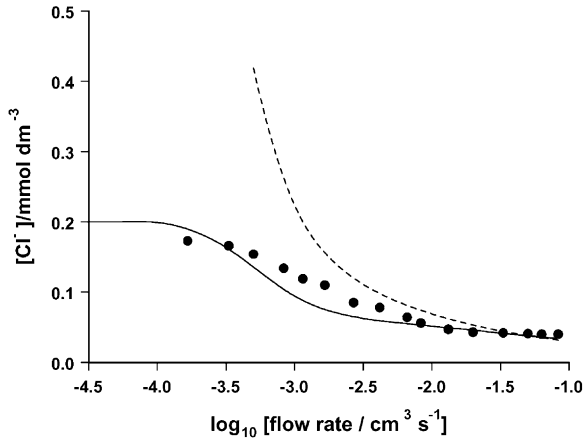

Fig. 7. [Cl^-] at the downstream detector electrode (●) as a function of $\log_{10}$ (flow rate) for 2.0×10^{-4} mol dm^{-3} 4-CP solution (oxygenated). The best fits are shown for the mixed-control model (solid line, with $k'_{MC} = 4.5 \times 10^{-10}$ mol cm^{-2} s^{-1}) and the surface-limited model (dashed line, with $k'_{SL} = 1.5 \times 10^{-10}$ mol cm^{-2} s^{-1}). Intensity of light = 7.2×10^{16} q cm^{-2} s^{-1}.

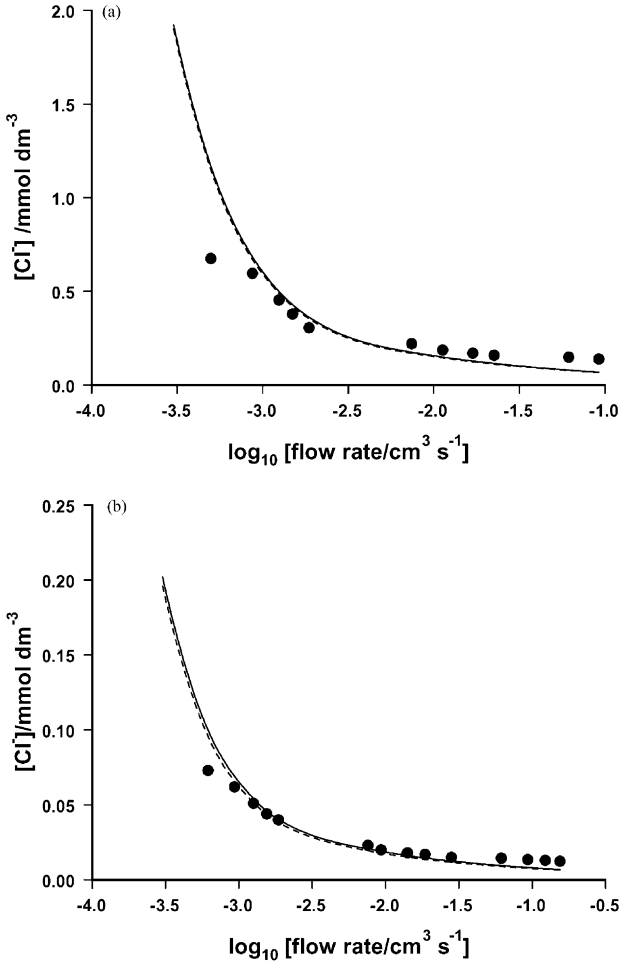

Fig. 8. [Cl^-] at the downstream detector electrode (●) as a function of $\log_{10}$ (flow rate) for (a) 5.0×10^{-3} mol dm^{-3} 4-CP solution (aerated) in the presence of 0.1 mol dm^{-3} $NaClO_4$ as supporting electrolyte. The best fits are shown for the models with $k'_{SL} = 2.8 \times 10^{-10}$ mol cm^{-2} s^{-1} and $k'_{MC} = 3.0 \times 10^{-10}$ mol cm^{-2} s^{-1} at a light intensity of 2.0×10^{17} q cm^{-2} s^{-1}. (b) 1.0×10^{-3} mol dm^{-3} 4-CP solution (aerated) in the presence of 0.1 mol dm^{-3} $NaClO_4$ as supporting electrolyte, with best fits to $k'_{SL} = 0.35 \times 10^{-10}$ mol cm^{-2} s^{-1} and $k'_{MC} = 0.45 \times 10^{-10}$ mol cm^{-2} s^{-1} at a light intensity of 1.0×10^{17} q cm^{-2} s^{-1}.

The respective light fluxes for these two cases were 2.0×10^{17} and 1.0×10^{17} q cm^{-2} s^{-1}. The reason for considering higher [4-CP]* was to investigate the influence of supporting electrolyte in controlling the surface kinetics of the degradation process under conditions where mass transport effects were expected (and confirmed) to be unimportant. The experimental data were compared alongside the best fits to the surface-limited models (for 5.0×10^{-3} mol dm^{-3} 4-CP, $k'_{MC} = 3.0 \times 10^{-10}$ mol cm^{-2} s^{-1} and $k'_{SL} = 2.8 \times 10^{-10}$ mol cm^{-2} s^{-1}; for 1.0×10^{-3} mol dm^{-3} 4-CP, $k'_{MC} = 0.45 \times 10^{-10}$ mol cm^{-2} s^{-1} and $k'_{SL} = 0.35 \times 10^{-10}$ mol cm^{-2} s^{-1}). In both cases, the experimental results conform to the model fairly well over the range of flow rates investigated, but the predicted rate constants are

comparatively low, indicating that the photomineralisation becomes less efficient under such conditions.

Comparison of rate constants obtained with and without supporting electrolyte for 5.0×10^{-3} mol dm^{-3} 4-CP clearly shows that the presence of supporting electrolyte diminishes the photomineralisation rate by a factor of ca. 2. The most plausible explanation for this behaviour is that the supporting electrolyte may inhibit the adsorption of chlorophenol and/or O_2 on the TiO_2 surface.

The effect of KNO_3 on the 4-CP-TiO_2-O_2 photosystem was demonstrated by Mills et al. [36], who found a gradual decrease in the rate of CO_2 formation with increase of [KNO_3], covering the range 0.01–1.0 mol dm^{-3}. More specifically, it was demonstrated that the presence of nitrate anion, at a concentration of ca. 0.4 mol dm^{-3}, could effectively reduce the rate of the photoprocess by a factor of 2. This effect was shown to be most likely due to the absorption of UV-light by KNO_3 in the range 300–360 nm, causing a variation in transmittance values. KNO_3 has also been used to control ionic strength in this system by Bahnemann's group [18]; they took care to demonstrate NO_3^- is essentially inert under these conditions.

In order to obtain information on the UV absorption characteristics of $NaClO_4$, UV spectra ($350 > \lambda > 200$ nm) were recorded for 0.1 mol dm^{-3} $NaClO_4$, 1.0×10^{-3} mol dm^{-3} 4-CP and 1.0×10^{-3} mol dm^{-3} 4-CP with 0.1 mol dm^{-3} $NaClO_4$. Comparison of these UV spectra confirmed Mills' conclusion [36] that $NaClO_4$ had virtually no effect on the UV absorption of 4-CP, and would also not partially screen the TiO_2 from irradiation under the conditions of the experiments reported herein. This observation led us to carry out further investigations on the effect of $NaClO_4$, employing a batch photoreactor with suspended TiO_2 where mass transport effects are completely negligible. Accordingly, a solution of 1.0×10^{-3} mol dm^{-3} 4-CP containing a suspension of 0.1% TiO_2 was photomineralised in the presence of 0.1 mol dm^{-3} $NaClO_4$ and without supporting electrolyte under aerated conditions at a light flux density of 2.4×10^{17} q cm^{-2} s^{-1}. Degradation kinetics were monitored (in situ) by recording the potential difference as a function of irradiation time, as described in the experimental section. Again, the faster rate of Cl^- formation observed (1.67×10^{-8} mol dm^{-3} s^{-1}) in the absence of supporting electrolyte, compared to that with supporting electrolyte (0.92×10^{-8} mol dm^{-3} s^{-1}) confirms the deductions of the CFMED measurements (Fig. 9).

As briefly highlighted above, the diminution of the photomineralisation kinetics with $NaClO_4$ present is most likely due to partial blockage of the active sites of the TiO_2 photocatalyst [37].

3.3. Photodegradation of 3- and 2-chlorophenols solutions via CFMED

Further assessment of the CFMED approach related to the photomineralisation of 3- and 2-CPs, considering the contribution of [O_2] (i.e. 0.2 and 1.0 atm O_2) and the presence of supporting electrolyte (under aerated conditions) in controlling the photomineralisation kinetics. Accordingly, a series of investigations were carried out at a light flux density of either 1.0×10^{17} or 1.2×10^{17} q cm^{-2} s^{-1} with the organic substrate at a concentration of 1.0×10^{-3} mol dm^{-3}.

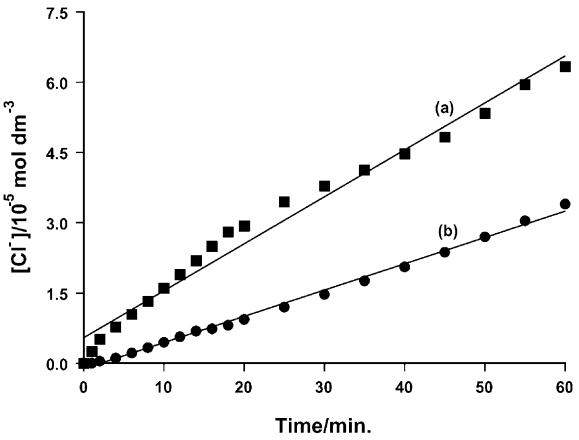

Fig. 9. [Cl^-] formation as a function of time during the photodegradation of 1.0×10^{-3} mol dm^{-3} 4-CP solution (aerated), without supporting electrolyte (a) and with 0.1 mol dm^{-3} $NaClO_4$ present (b).

Fig. 10a and b for 1.0×10^{-3} mol dm^{-3} 2-CP solutions with a light flux of 1.2×10^{17} q cm^{-2} s^{-1} (aerated and oxygenated, respectively) clearly show that both models provide a reasonable description of the data, but at slow flow rates, the mixed-control model is optimal. Similar behaviour was found for 3-CP solutions under both aerated and oxygenated conditions.

The faster mineralisation kinetics of oxygenated 2-CP ($k'_{MC} = 3.6 \times 10^{-10}$ mol cm^{-2} s^{-1}), compared to the aerated condition ($k'_{MC} = 2.1 \times 10^{-10}$ mol cm^{-2} s^{-1}), follows a similar trend already identified for 4-CP.

The photomineralisation kinetics of 2- and 3-CPs in the presence of 0.1 mol dm^{-3} $NaClO_4$ as supporting electrolyte were found to fit the theoretical models reasonably well. With a light flux of 1.0×10^{17} q cm^{-2} s^{-1}, the values of k'_{MC} (0.65×10^{-10} mol cm^{-2} s^{-1} for 3-CP and 0.53×10^{-10} mol cm^{-2} s^{-1} for 2-CP and k'_{SL} (0.40×10^{-10} mol cm^{-2} s^{-1} for both CPs) are consistent with the result obtained for 1.0×10^{-3} mol dm^{-3} 4-CP with 0.1 mol dm^{-3} $NaClO_4$ (Fig. 8b) at the same light flux. These results clearly indicate again that the presence of $NaClO_4$ as supporting electrolyte dramatically reduces the photomineralisation rate.

3.4. Photodegradation of 2,4-dichlorophenol (2,4-DCP) solutions via CFMED

Having successfully investigated the degradation profiles of monochlorophenols, particularly elucidating the role of mass transport in controlling the overall kinetics,

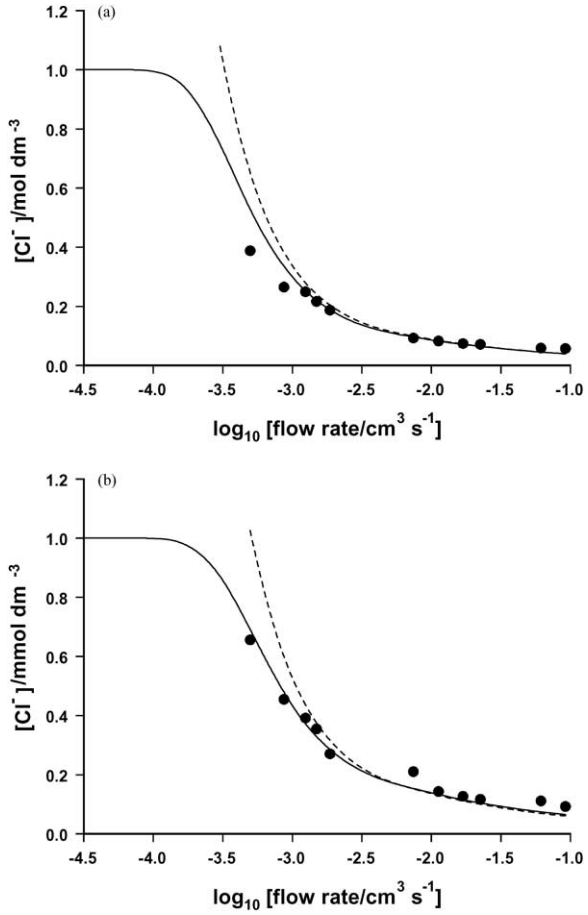

Fig. 10. $[Cl^-]$ at the downstream detector electrode (●) as a function of $\log_{10}$ (flow rate) with a light flux density of 1.2×10^{17} q cm^{-2} s^{-1} for (a) 1.0×10^{-3} mol dm^{-3} 2-CP solution (aerated). The best fits are shown for the mixed-control model (solid line, with $k'_{MC} = 2.1 \times 10^{-10}$ mol cm^{-2} s^{-1}) and the surface-limited model (dashed line, with $k'_{SL} = 1.6 \times 10^{-10}$ mol cm^{-2} s^{-1}). (b) 1.0×10^{-3} mol dm^{-3} 2-CP solution (oxygenated), with best fits for the mixed-control model (solid line, with $k'_{MC} = 3.6 \times 10^{-10}$ mol cm^{-2} s^{-1}) and the surface-limited model (dashed line, with $k'_{SL} = 2.5 \times 10^{-10}$ mol cm^{-2} s^{-1}).

the application of CFMED was extended briefly to the photomineralisation of 2,4-DCP under aerated conditions.

Following the earlier approach on the investigation of the effect of light flux on the photomineralisation kinetics of 4-CP (Section 3.2.2), our first objective was confined to an investigation of this effect on 1.0×10^{-3} mol dm^{-3} 2,4-DCP at applied light fluxes of 1.7×10^{17} and 1.0×10^{17} q cm^{-2} s^{-1}. The observed $[Cl^-]$ — flow rate profiles were found to be best analysed with the mixed-control model, over the whole range of flow rates investigated, with the rate constants cited in Table 3. These data again imply that under aerated conditions the kinetics of the photoprocess are closely proportional to the effective light flux, as found for 4-CP.

Finally, it is useful to assess the effect of supporting electrolyte in the photodegradation of 2,4-DCP. The resulting analysis of data obtained on an aerated solution of 1.0×10^{-3} mol dm^{-3} 2,4-DCP with 0.1 mol dm^{-3} $NaClO_4$, illuminated at an intensity of 1.0×10^{17} q cm^{-2} s^{-1}, yielded a rate constant $k'_{MC} = 1.0 \times 10^{-10}$ mol cm^{-2} s^{-1} (or $k'_{SL} = 0.8 \times 10^{-10}$ mol cm^{-2} s^{-1} since mass transport effects were negligible). The results again support the conclusion (Section 3.2.4) that the mineralisation rate is significantly influenced by added supporting electrolyte and that the diminished interfacial fluxes make mass transport of 2,4-DCP less significant.

3.5. Quantum efficiency

It is informative to estimate the quantum efficiency of the photoprocesses studied in the CFMED system. The quantum yield is flow rate dependent, attaining a maximum value when mass transport is sufficiently high to be unimportant. At the high flow rate limit, the apparent quantum efficiency of the photomineralisation process can be calculated via

$$\text{Quantum efficiency} = \frac{k''_{SL} N_A}{\Phi_{LFD}} \quad (20)$$

where N_A is Avogadro's number, Φ_{LFD} the light flux density (q cm^{-2} s^{-1}), and k''_{SL} can be calculated from Eq. (18).

The degradation processes described in this study correspond to reasonable values of the quantum yields in the range 0.1–0.2% for all the CPs studied without supporting electrolyte present. These values match with the range of quantum yields 0.1–1.0%, reviewed by Mills and Le Hunte [1]. Within experimental error, there are no significant effects of the position of the Cl atom on the overall kinetics and the quantum yield of the process. Most notably, the quantum efficiency of the photocatalytic reactions of 4-CP and 2-CP increased when the O_2 level was increased to saturated conditions (1 atm O_2) compared to aerated solution, in good agreement with studies carried out mainly in suspension [2]. With supporting electrolyte, the quantum yield is diminished for the reasons discussed earlier.

Table 3
Values of k'_{MC} and k'_{SL} for photomineralisation of 2,4-DCP

[2,4-DCP] (mol dm^{-3})	[$NaClO_4$] (mol dm^{-3})	Light flux density (q cm^{-2} s^{-1})	k'_{MC} (mol cm^{-2} s^{-1})
1.00×10^{-3}	0.0	1.7×10^{17}	3.0×10^{-10}
1.00×10^{-3}	0.0	1.0×10^{17}	2.0×10^{-10}
1.00×10^{-3}	0.1	1.0×10^{17}	1.0×10^{-10}

4. Conclusions

CFMED has been shown to be a successful approach to studying the photodegradation kinetics of various chlorophenol compounds, allowing the contribution of surface kinetics and mass transport effects to be readily identified. Mass transport has been shown to be a key parameter in controlling photomineralisation rates, particularly with low substrate concentrations. Additionally, the rate of photomineralisation has been shown to be closely proportional to the light flux intensity. The effect of $NaClO_4$ supporting electrolyte is to impede the photomineralisation process, whereas an increasing concentration of oxygen in solution serves to enhance the photomineralisation rate.

It is useful to identify when mass transport will be important, generally compared to surface kinetics. For a given light intensity and oxygen level (assuming depletion effects are negligible), the key parameters are the effective mass transfer coefficient, k_T, and the bulk concentration of 4-CP. For dilute solutions, where $K_{CP}[\text{4-CP}] \ll 1$, it may be concluded from the present studies that mass transport will be important when $k_T < k'_{MC} K_{CP}$. Under the conditions of the experiments described in this paper, the latter product has a value in the range 7.0×10^{-4}–2.2×10^{-3} cm s^{-1}.

Although the mixed-control model developed in this paper provides a reasonable description of the photomineralisation process, it is also likely that O_2 depletion will become important at the slowest flow rates, which has not been considered. Refinement of the theoretical modelling, including the possibility of O_2 depletion may provide further insight into the factors governing the kinetics of photomineralisation process. Information is needed on O_2 photoreduction at immobilised TiO_2 surfaces and work in this direction is ongoing in our group [38].

Acknowledgements

S. Ahmed thanks the Ministry of Science and Technology, Government of Bangladesh, for a scholarship. We appreciate helpful advice and assistance from Phil Dobson, Nick Evans, Claire Jones, Julie Macpherson and Chris Slevin.

References

[1] A. Mills, S. Le Hunte, J. Photochem. Photobiol. A: Chem. 108 (1997) 1.
[2] A. Mills, R.H. Davies, D. Worsley, Chem. Soc. Rev. 22 (1993) 417.
[3] A.L. Linsbigler, G. Lu, J.T. Yates Jr., Chem. Rev. 95 (1995) 735.
[4] H.D. Burrows, L.S. Ernestova, T.J. Kemp, Yu.I. Skurlatov, A.P. Purmal, A.N. Yermakov, Prog. React. Kinet. 23 (1998) 145.
[5] M.I. Litter, Appl. Catal. B: Environmental 23 (1999) 89.
[6] J. Cunningham, P. Sedlak, J. Photochem. Photobiol. A: Chem. 77 (1994) 255.
[7] J.C. D'Oliveira, C. Minero, E. Pelizzetti, P. Pichat, J. Photochem. Photobiol. A: Chem.72 (1993) 261.
[8] K. Okamoto, Y. Yamamoto, H. Tanaka, M. Tanaka, A. Itaya, Bull. Chem. Soc. Jpn. 58 (1985) 2015.
[9] L. Rideh, A. Wehrer, D. Ronze, A. Zoulalian, Ind. Eng. Chem. Res. 36 (1997) 4712.
[10] M. Bideau, B. Claudel, C. Dubien, L. Faure, H. Kazouan, J. Photochem. Photobiol. 91 (1995) 137.
[11] H. El-Ekabi, N. Serpone, J. Phys. Chem. 92 (1998) 5726.
[12] A. Heller, Acc. Chem. Res. 28 (1995) 503.
[13] J.A. Byrne, B.R. Eggins, N.M.D. Brown, B. McKinney, M. Rouse, Appl. Catal. B. Environmental 17 (1998) 25.
[14] K. Okamoto, Y. Yamamoto, H. Hanaka, A. Itaya, Bull. Chem. Soc. Jpn. 58 (1985) 2023.
[15] T.A. Egerton, C.J. King, J. Oil Col. Chem. 62 (1979) 386.
[16] L. Vincze, T.J. Kemp, J. Photochem. Photobiol. A: Chem. 87 (1995) 257.
[17] L. Vincze, T.J. Kemp, P.R. Unwin, J. Photochem. Photobiol. A: Chem. 123 (1999) 7.
[18] J. Theurich, M. Lindner, D.W. Bahnemann, Langmuir 12 (1996) 6368.
[19] A. Mills, J. Wang, J. Photochem. Photobiol. A: Chem. 118 (1998) 53.
[20] S. Ahmed, C.E. Jones, T.J. Kemp, P.R. Unwin, Phys. Chem. Chem. Phys. 1 (1999) 5229.
[21] C.S. Turchi, D.F. Ollis, J. Phys. Chem. 92 (1988) 6852.
[22] A. Mills, J. Wang, Int. J. Res. Phys. Chem. Chem. Phys. 213 (1999) 49.
[23] A. Mills, D. Worsley, R.H. Davies, J. Chem. Soc., Chem. Commun. (1994) 2677.
[24] C.G. Hatchard, C.A. Parker, Proc. R. Soc. London, Ser. A 235 (1956) 518.
[25] R.G. Compton, P.R. Unwin, Philos. Trans. R. Soc. London, Ser. A 330 (1990) 1.
[26] R.G. Compton, C.A. Brown, J. Colloid Interface Sci. 165 (1994) 445.
[27] C.A. Brown, R.G. Compton, C.A. Narramore, J. Colloid Interface Sci. 160 (1993) 1517.
[28] F. Serra, M. Trillas, J. Garcia, X. Domenech, J. Environ. Sci. Health A 29 (1994) 1409.
[29] A. Mills, S. Morris, J. Photochem. Photobiol. A: Chem. 71 (1993) 75.
[30] Yu.I. Skurlatov, L.S. Ernestova, E.V. Vichutinskaya, D.P. Samsonov, I.V. Semenova, I.Ya. Rod'ko, V.O. Shvidky, R.I. Pervunina, T.J. Kemp, J. Photochem. Photobiol. A: Chem. 107 (1997) 207.
[31] J.S. Newman, Electrochemical Systems, Prentice-Hall, Englewood Cliffs, NJ, 1991.
[32] C.R. Wilke, P. Chang, AIChE J. 1 (1955) 264.
[33] R.W. Matthews, J. Catal. 111 (1988) 264.
[34] J.-C. D'Oliviera, G. Al-Sayyed, P. Pichat, Environ. Sci.-Technol. 24 (1990) 990.
[35] L. Rideh, A. Wehrer, D. Ronze, A. Zoulalian, Catal. Today 48 (1999) 357.
[36] A. Mills, S. Morris, R. Davies, J. Photochem. Photobiol. A: Chem. 70 (1993) 183.
[37] M. Abdullah, G.K.-C. Low, R.W. Matthews, J. Phys. Chem. 94 (1990) 6820.
[38] S. Ahmed, T.J. Kemp, P.R. Unwin, J. Phys. Chem., to be submitted (2001).